

Time-lapse FWI prediction of CO₂ saturation and pore pressure

Qi Hu and Kristopher A. Innanen

ABSTRACT

The estimation of CO₂ saturation and pore pressure from time-lapse seismic data requires a physical model relating the variations in reservoir properties to the changes in seismic attributes. We propose a complete rock physics workflow combining Macbeth's model and Gassmann's equations to predict elastic properties as a function of porosity, mineralogy, saturation and pressure. We validate this workflow using a published dataset. In particular, we demonstrate the advantages of Macbeth's model in predicting the effect of pressure changes. Furthermore, we propose a full waveform inversion (FWI) algorithm incorporating the proposed model for the prediction of the time-evolution of CO₂ saturation and pore pressure. This approach allows for direct updating of reservoir properties from seismic data. We derive static rock properties, such as porosity and clay content, from baseline data and use them as input to predict dynamic reservoir properties (saturation and pressure) from monitor data. We illustrate the potential of the approach using a synthetic time-lapse dataset.

INTRODUCTION

An important technology supporting reduction of greenhouse gas emissions is the geological storage of carbon dioxide (Davis et al., 2019; Ringrose, 2020; Pörtner et al., 2022); for instance, deep saline aquifers have been identified as promising sites for CO₂ storage. Time-lapse seismic surveys provide a monitoring mode in which migration and distribution of the injected CO₂ can be tracked, and leakage problems if any can be identified (Arts et al., 2003; Chadwick et al., 2005). Ideally, for reliable conformance verification, quantitative estimates/maps of CO₂ saturation would be produced by such technology, to be compared against reservoir modeling predictions (Dupuy et al., 2021).

The estimation of saturation and pressure from seismic data requires a physical model relating the variations in reservoir properties to the changes in seismic response. The saturation effect can be generally described by Gassmann's equation combined with the density equation (Mavko et al., 2020; Grana et al., 2021). Typically, if CO₂ replaces water, the P-wave velocity and density of the saturated rock decrease, whereas the S-wave velocity increases. The pressure dependence of velocities has been described by several empirical equations (Han, 1987; Eberhart-Phillips et al., 1989; Landrø, 2001; Jones, 1995; Sayers, 2006). Generally, if effective pressure increases, both P- and S-wave velocities of the rock increase, whereas the pressure effect on density is often negligible unless the rock experiences a severe compaction. The increase in velocity is more significant at low effective pressure than high effective pressure. Indeed, many models are based on exponential relations that tend to an asymptotic value at high pressure.

MacBeth (2004) proposed an analogous equation to link dry-rock elastic moduli to effective pressure with an exponential equation by fitting a set of lab measurements conducted on sand and shaly-sand dry samples. The pressure dependence of dry-rock properties in-

cluding porosity and lithology effects have also been reported (Saul and Lumley, 2013; Grana, 2016). These relations can be directly integrated in rock physics models used in reservoir characterization to describe dry-rock elastic moduli as a function of effective pressure, the effect of fluid being then modeled by Gassmann's equation.

The rock physics model can be combined with full waveform inversion, which has the capacity to produce high-resolution elastic parameter models (e.g., velocity, density, and modulus), for quantitative characterization and monitoring of reservoir properties. This is generally implemented using a two-step inversion algorithm, in which an elastic FWI prediction of elastic properties is followed by rock physics inversion (Bosch et al., 2010; Queißer and Singh, 2013; Dupuy et al., 2021). Hu et al. (2021) formulated a direct procedure for updating rock and fluid properties within elastic FWI. They achieve this by re-parameterizing the inversion in terms of rock physics properties using the chain rule. The main advantages of this approach are: 1) it allows examination of any rock physics property that has a well-defined relationship with elastic parameters; 2) it shares the same numerical structure as the conventional FWI, and 3) with a suitable initial model, the method exhibits higher prediction accuracy than conventional two-step approaches. Hu et al. (2022) extended the approach to predict CO₂ saturation from time-lapse seismic data. However, this approach is only applicable to the cases where the effect of pressure changes on elastic properties is negligible.

In this work, we first review MacBeth (2004) pressure model and its variant which includes porosity and lithology effects (Grana, 2016), introduce the complete rock physics workflow for modeling saturation-pressure changes, and describe how to incorporate this model into the time-lapse FWI framework of Hu et al. (2022). We then systematically examine the response of the inversion to a synthetic time-lapse dataset.

METHODOLOGY

Considerations for the rock physics model

In order to estimate variations in dynamic properties (e.g., CO₂ saturation and pore pressure) from time-lapse seismic data, a physical relation between saturation and pressure and elastic properties must be established. With the fluid effect at seismic frequency being well described by Gassmann's equations, the main challenge lies in the description of pressure within the rock physics model.

We first introduce the definitions about the different pressures considered in this work. Pore pressure P_p , also known as formation pressure, is the in-situ pressure of the fluids in the pores. When the pore pressure is hydrostatic, we have

$$P_p = \rho_w g z, \quad (1)$$

where z is the depth, g is the acceleration of gravity, and ρ_w is the density of water. The confining or overburden pressure P_c results from the weight of overlying sediments and is generally obtained by integrating the density log:

$$P_c = g \int_0^z \rho(z') dz', \quad (2)$$

where ρ is the bulk density of the rock. The effective pressure P_e is defined as the difference between overburden pressure and pore pressure:

$$P_e = P_c - \eta P_p, \quad (3)$$

where $0 \leq \eta \leq 1$ is the effective stress coefficient. In the following, we assume for simplicity that η is equal to 1.

The effective pressure dependence of velocity has been extensively studied by geophysicists because of the direct and visible impact of effective pressure on rock frame properties, whereas pore pressure is a very important parameter with respect to reservoir engineering. In this work, we assume the overburden pressure to be known, so the effective pressure and pore pressure are interchangeable.

MacBeth's pressure model

MacBeth (2004) proposed an analogous equation to link dry-rock bulk modulus to effective pressure using an exponential relation:

$$K_{\text{dry}}(P_e) = \frac{K^\infty}{1 + A_K e^{-\frac{P_e}{P_K}}}, \quad (4)$$

where K^∞ , A_K , and P_K are empirical parameters: K^∞ represents the asymptotic value as effective pressure increases, whereas A_K and P_K are related to the curvature. Grana (2004) illustrated that K^∞ and A_K are not independent if the dry-rock modulus K_0 at a given effective pressure P_0 is known, and modified Equation 1 to include dependence on porosity ϕ and clay content V_{clay} :

$$K_{\text{dry}}(P_e) = \frac{K^\infty}{1 + \frac{K^\infty - K_0}{K_0} e^{-\frac{P_{\text{eff}} - P_0}{P_K}}}; \quad (5)$$

$$K^\infty = \lambda_1(\phi + aV_{\text{clay}}) + \lambda_2, \quad (6)$$

where a , λ_1 , and λ_2 are empirical parameters that must be fitted using lab measurements. Datasets from literature or from nearby fields could be used to integrate the available core samples, as long as the observed pressure effect on elastic properties has the same behavior. Similar results have been obtained for the shear modulus:

$$\mu_{\text{dry}}(P_{\text{eff}}) = \frac{\mu^\infty}{1 + \frac{\mu^\infty - \mu_0}{\mu_0} e^{-\frac{P_e - P_0}{P_\mu}}}; \quad (7)$$

$$\mu^\infty = \lambda_3(\phi + aV_{\text{clay}}) + \lambda_4, \quad (8)$$

where μ_0 is the dry-rock shear modulus at effective pressure P_0 ; λ_3 and λ_4 are empirical parameters.

The MacBeth's relations focus on the effect of pressure on elastic properties and are lack of physics to account for the effect of rock properties, such as porosity and lithology.

By contrast, the conventional Hertz-Mindlin based models, although have a pressure term in their expressions, are classically used to predict static rock properties rather than pressure changes. To combine the advantages of both, we calculate the initial/baseline dry-rock moduli, namely K_0 and μ_0 , using the Hertz-Mindlin equations, then apply the pressure effect in the monitor stage using the modified MacBeth's equation (Equations 5-8).

Complete rock physics workflow

We calculate the saturated-rock elastic moduli by combining the dry-rock elastic moduli, the elastic moduli of the solid and fluid phases, and the measured porosity and by applying Gassmann's equation, according to the insitu reservoir conditions. The equations are given here with underlined dependencies to pore pressure P_p and CO₂ saturation S_{CO_2} :

$$K_{\text{sat}}(S_{\text{CO}_2}, P_p) = K_{\text{dry}}(P_p) + \frac{[1 - K_{\text{dry}}(P_p)/K_m]^2}{\phi/K_f(S_{\text{CO}_2}, P_p) + (1 - \phi)/K_m - K_{\text{dry}}(P_p)/K_m^2}, \quad (9)$$

$$\mu_{\text{sat}}(P_p) = \mu_{\text{dry}}(P_p), \quad (10)$$

$$\rho_{\text{sat}}(S_{\text{CO}_2}, P_p) = (1 - \phi)\rho_m + \phi\rho_f(S_{\text{CO}_2}, P_p), \quad (11)$$

where the subscripts $m, f, \text{dry}, \text{sat}$ indicate solid matrix, fluid phase, dry rock, and saturated rock, respectively.

The elastic moduli of the solid matrix are computed using Voigt-Reuss-Hill average for a mixture of quartz and clay. The elastic properties of the fluid components (water and CO₂) depend on reservoir conditions, such as temperature and pore pressure, as well as on the fluid composition and characteristics. We first compute the density and bulk modulus of each fluid component using the Batzle and Wang (1992) equations, then compute the bulk modulus of the fluid mixture using the Brie et al. (1995) equation, assuming patchy saturation. In Figure 1, the complete rock physics workflow is summarized.

Steps of rock physics modeling		
Solid phase:	$K_m = f(K_q, K_c, V_{\text{clay}})$	Voigt-Reuss-Hill
Fluid phase:	$K_{\text{CO}_2, w} = f(T, P_p)$ $K_f = f(K_{\text{CO}_2}, K_w, S_{\text{CO}_2})$	Batzle-Wang Brie
Dry rock:	$K_{\text{dry}}(P_0) = f(K_m, \phi, P_0)$ $K_{\text{dry}}(P_{\text{eff}}) = K_{\text{dry}}(P_0) + f(P_{\text{eff}} - P_0)$	Hertz-Mindlin MacBeth
Saturated rock:	$K_{\text{sat}} = f(K_m, K_f, K_{\text{dry}}, \phi)$	Gassmann
	$(V_P, V_S, \rho) = f(\phi, V_{\text{clay}}, S_{\text{CO}_2}, P_p)$	

FIG. 1. The complete rock physics workflow we propose to link static rock properties (porosity and lithology) and dynamic reservoir properties (CO₂ saturation and pore pressure) to seismic attributes.

Model calibration

Here we take three core samples from Han’s dataset to illustrate how to calibrate our rock physics model in practical applications. Our goal is to calibrate the model so that it can accurately predict velocity as a function of porosity, clay content, and effective pressure.

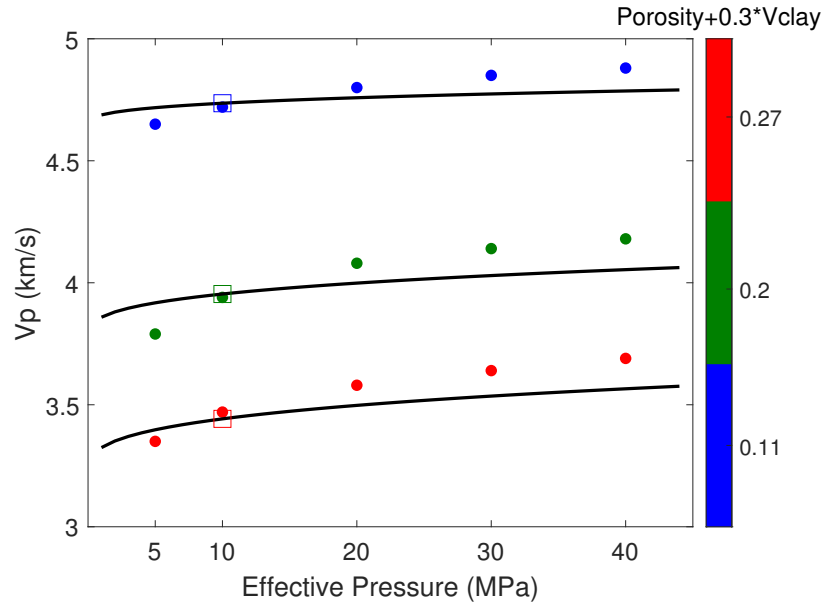


FIG. 2. Calibration of rock physics model using Han’s dataset (subset of 3 samples). The Hertz-Mindlin model is combined with Gassmann’s equations to predict saturated-rock velocity as a function of effective pressure including porosity and mineralogy effects. The model is calibrated using baseline data with pressure 10 MPa, then automatically predicts the data at 5,20,30,40 MPa.

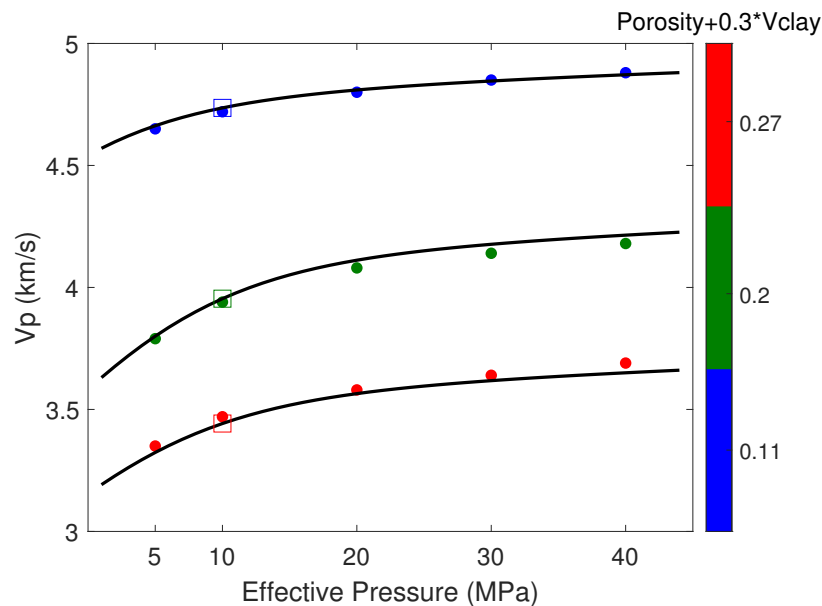


FIG. 3. Macbeth’s relation combined with Gassmann’s equations to predict saturated-rock velocity as a function of effective pressure including porosity and mineralogy effects. The predicted data with Hertz-Mindlin equations at pressure 10 MPa are used as input in Macbeth’s model.

We assume that the initial or baseline pressure is 10 MPa, and that the data at other pressures correspond to the monitor survey. We first examine the model which uses the Hertz-Mindlin equation only. This means once we calibrate the model at the initial pressure, the model automatically predicts the value at future pressures. Figure 2 shows that the Hertz-Mindlin equation, which has a cubic root of effective pressure in its expression, does not correctly approximate the nonlinear behavior of velocity due to pressure changes. The main advantages of the proposed model, which combines the Hertz-Mindlin and the Macbeth's equations, are the exponential trend and the inclusion of empirical parameters that we can calibrate to match the observations. Indeed, we observe a close match between the predicted data and the true ones using the proposed model (Figure 3).

Time-lapse FWI strategy

We propose to combine the proposed rock physics model with the FWI algorithm set out by Hu et al. (2021) to achieve a direct and joint estimation of CO₂ saturation and pore pressure from time-lapse seismic data.

First, we apply the rock physics FWI approach to the baseline (pre-injection) data for the estimation of static rock properties, e.g., porosity and clay content; then, we use the same inverse method and use the inverted baseline models as prior knowledge (fixed values) to estimate the dynamic properties from monitor (post-injection) data. The objective function for baseline model reconstruction is expressed as

$$E_b = \left\| \mathbf{d}_{\text{obs}_b}(\phi^t, V_{\text{clay}}^t) - \mathbf{d}_{\text{syn}_b}(\phi, V_{\text{clay}}) \right\|^2, \quad (12)$$

where $\mathbf{d}_{\text{obs}_b}$ and $\mathbf{d}_{\text{syn}_b}$ denote the observed and synthetic baseline data, respectively. ϕ^t and V_{clay}^t denote the true porosity and clay content models. The baseline CO₂ saturation and pressure condition are assumed to be known. The goal is to recover the ϕ and V_{clay} models by iteratively minimizing the difference between $\mathbf{d}_{\text{obs}_b}$ and $\mathbf{d}_{\text{syn}_b}$.

The objective function for monitor model reconstruction is

$$E_m = \left\| \mathbf{d}_{\text{obs}_m}(\phi^t, V_{\text{clay}}^t, S_{\text{co2}}^t, P_p^t) - \mathbf{d}_{\text{syn}_m}(\phi^b, V_{\text{clay}}^b, S_{\text{co2}}, P_p) \right\|^2, \quad (13)$$

where $\mathbf{d}_{\text{obs}_m}$ and $\mathbf{d}_{\text{syn}_m}$ are the observed and synthetic monitor data, respectively. ϕ^b and V_{clay}^b are the inverted porosity and clay content models from the baseline survey. They are not updated in the monitor stage. The goal is to recover the saturation model S_{co2} and pressure model P_p by iteratively minimizing the difference between $\mathbf{d}_{\text{obs}_m}$ and $\mathbf{d}_{\text{syn}_m}$.

NUMERICAL EXAMPLE

We apply the proposed approach to a synthetic model as shown in Figure 4. The initial CO₂ saturation is 0 everywhere and the initial pore pressure is hydrostatic. The two models then change locally due to the injection of CO₂ at 500 m depth and 500 m position. In this simulation, we neglect the uncertainty associated with the baseline model reconstruction, namely, we consider two model unknowns only: the monitor model of CO₂ saturation and pore pressure. Figure 5 illustrates the details of the pressure model, in which we consider a clear pressure build-up due to the injection.

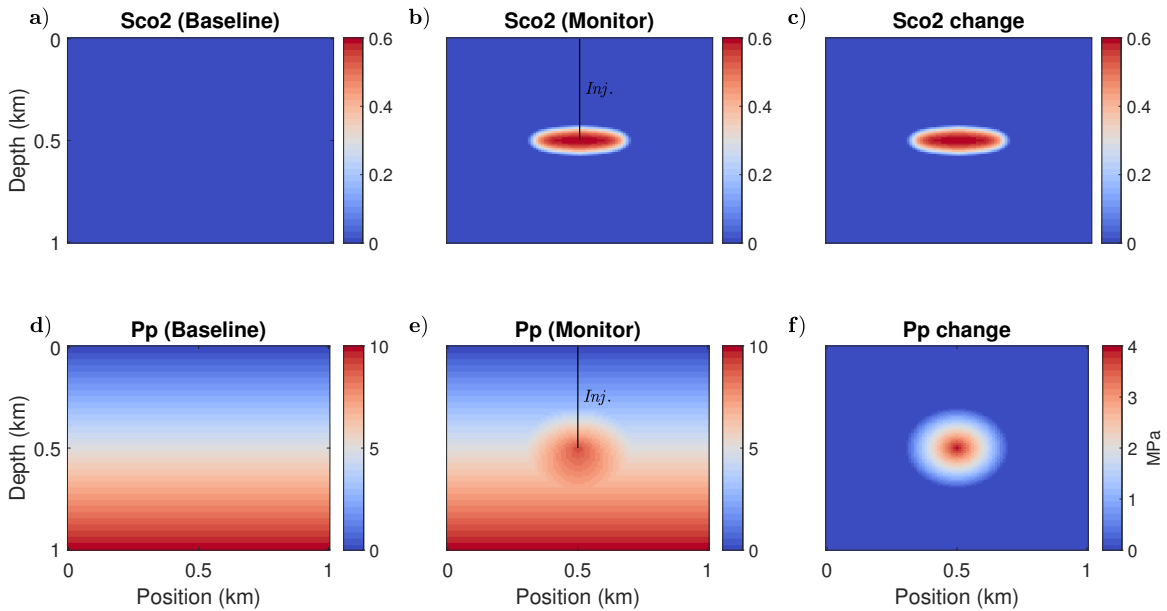


FIG. 4. True baseline, monitor, and time-lapse models of CO₂ saturation and pore pressure. The black line indicates the location of the injection well.

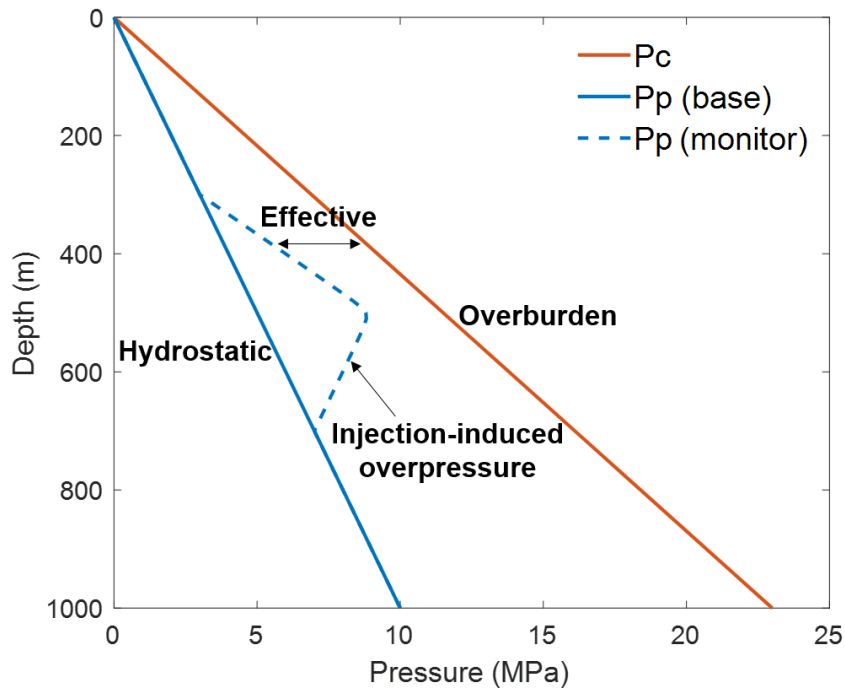


FIG. 5. Details of the pressure model.

In Figure 6, we compute the theoretical curves of velocities and density as a function of CO₂ saturation and pore pressure based on the rock physics model, according to the parameter values of the synthetic model. The results are consistent with existing studies: if CO₂ saturation increases, the P-wave velocity and density decrease, whereas the S-wave velocity slightly increases; both P- and S-wave velocities decrease as pore pressure increases,

whereas the pressure effect on density is negligible. We note that there are two factors leading to the significant velocity changes: 1) by adopting the proposed rock physics model, we assume weakly consolidated rocks; 2) the depth range we use corresponds to low pressure values, as compared to many studies where the reservoir is located at a deeper location.

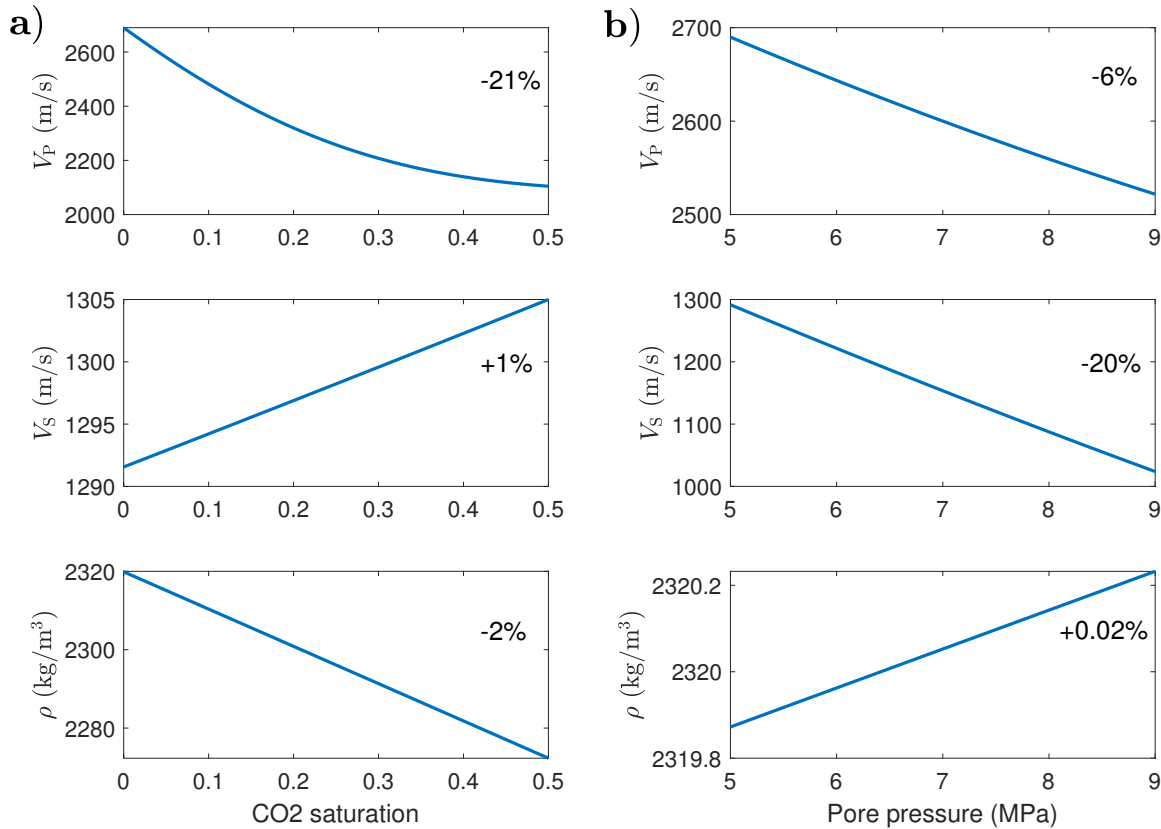


FIG. 6. Theoretical curves of the proposed rock physics model: P-wave velocity, S-wave velocity, and density versus (a) CO₂ saturation and (b) pore pressure.

In Figure 7, we plot the velocity and density models corresponding to the rock property model. The time-lapse elastic changes are consistent with the analysis in Figure 6. Consequently, we observe clear time-lapse events in the noise-free synthetic data (Figure 8). For the inversion test, we apply the 2D frequency-domain rock-physics FWI algorithm (Hu et al., 2021), using a multiscale approach (Bunks et al., 1995; Brossier et al., 2009; Keating and Innanen, 2019) by successively inverting slightly overlapping frequency groups. The truncated Gauss-Newton optimization method (Métivier et al., 2017) is used.

The recovered monitor model of CO₂ saturation and pore pressure shows a good agreement with the true one (Figure 9). The parameter crosstalk is weak. We attribute this to the fact that the two properties have very different sensitivities with respect to the P- and S-wave velocities (Figure 6). In Figure 10, the convergence properties of the inversion are summarized. We start iterations at low frequencies to prevent convergence of the objective function toward local minima, then slowly introduce higher frequencies to image fine structures. The objective function has a sudden increase when entering into a next frequency group, but decreases efficiently after model updating. The solutions are examined via the

relative model error. We observe the convergence characteristics of a reliable inversion.

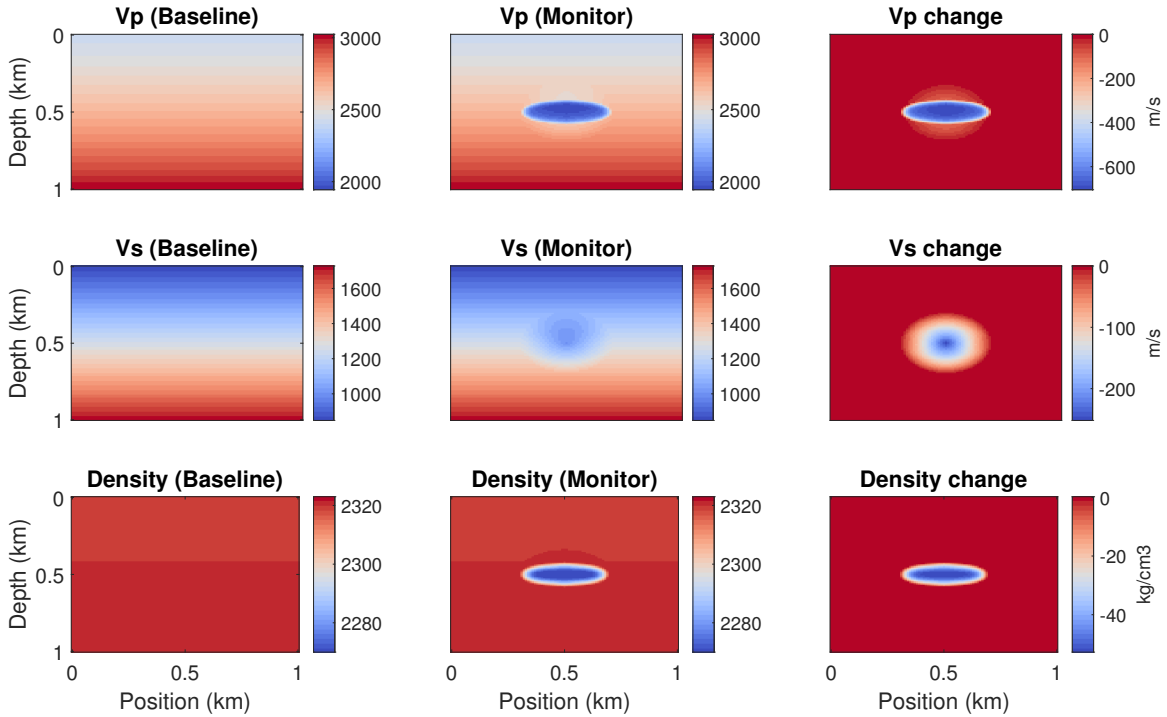


FIG. 7. True baseline, monitor, and time-lapse models of P-wave velocity, S-wave velocity, and density.

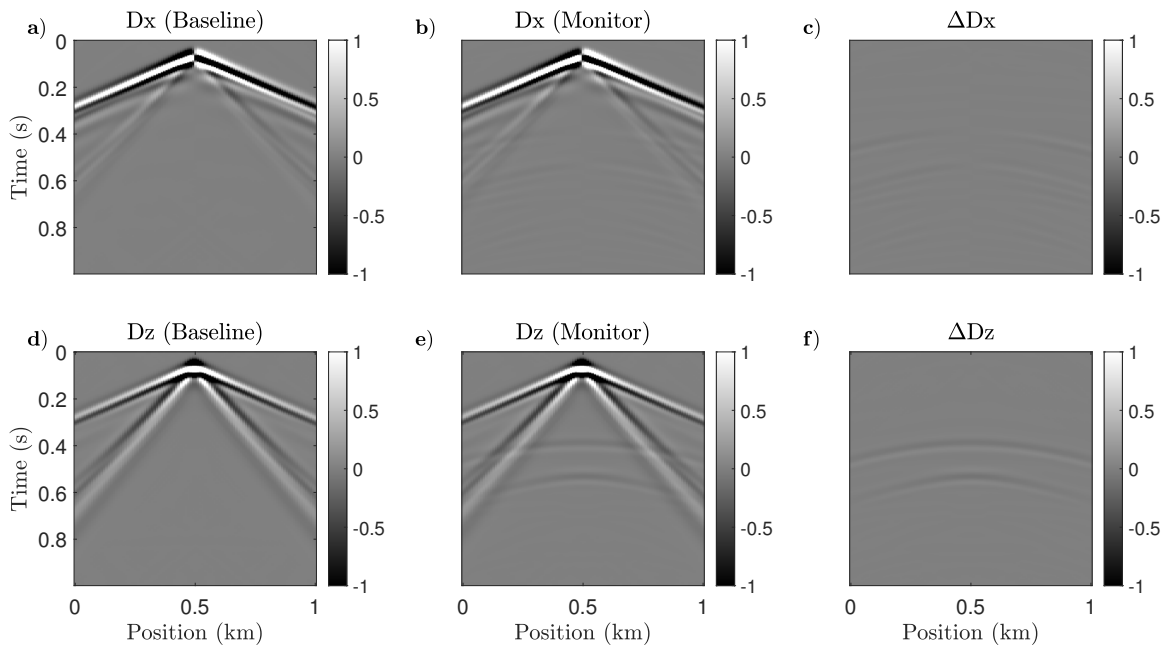


FIG. 8. Baseline, monitor, and differential seismograms (Horizontal and vertical displacements) computed for the true model. Ricker wavelet source with a central frequency of 15 Hz is used.

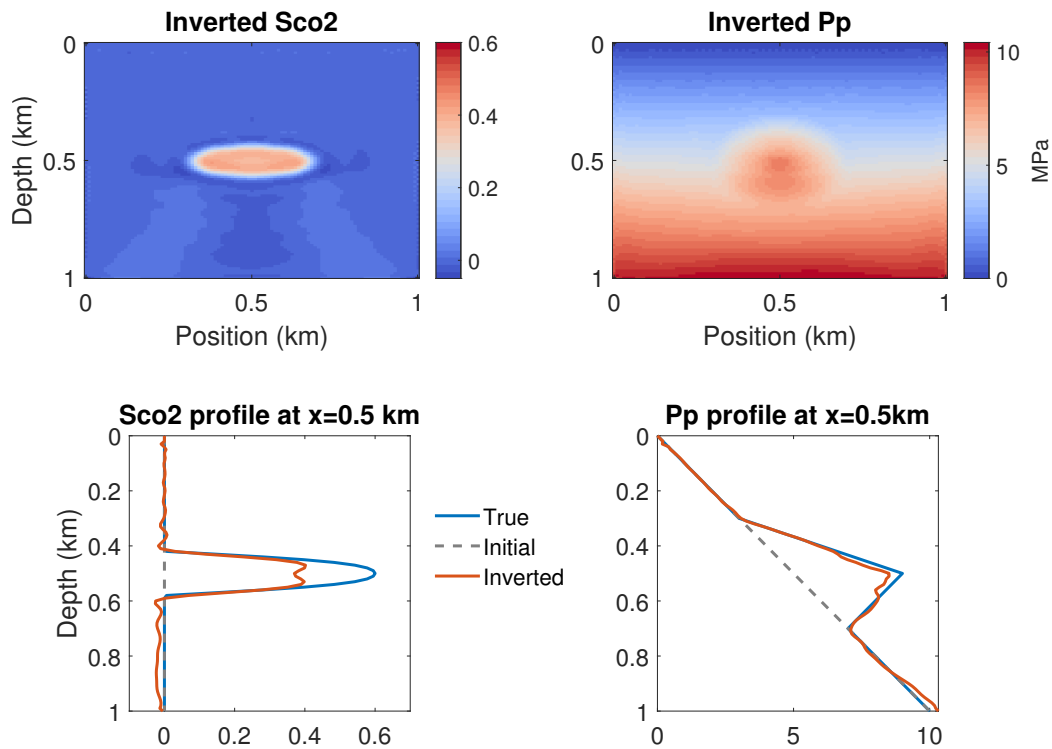


FIG. 9. Recovered monitor model of CO₂ saturation and pore pressure.

CONCLUSIONS

We have proposed a complete rock physics workflow for modeling saturation-pressure changes. A critical step in this workflow is the use of Macbeth’s model to account for the pressure effect on dry-rock elastic moduli. We then propose an FWI algorithm incorporating the proposed rock physics model for the quantitative prediction of CO₂ saturation and pore pressure from time-lapse seismic data. We demonstrate the effectiveness of this approach using a synthetic time-lapse dataset. Examination of complex geological models and uncertainties associated with the rock physics model, the observed data, and the baseline inversion result are important steps in moving this research forward.

ACKNOWLEDGMENTS

We thank the sponsors of CREWES for continued support. This work was funded by CREWES industrial sponsors and NSERC (Natural Science and Engineering Research Council of Canada) through the grant CRDPJ 543578-19. The first author was partially supported by a scholarship from the SEG Foundation.

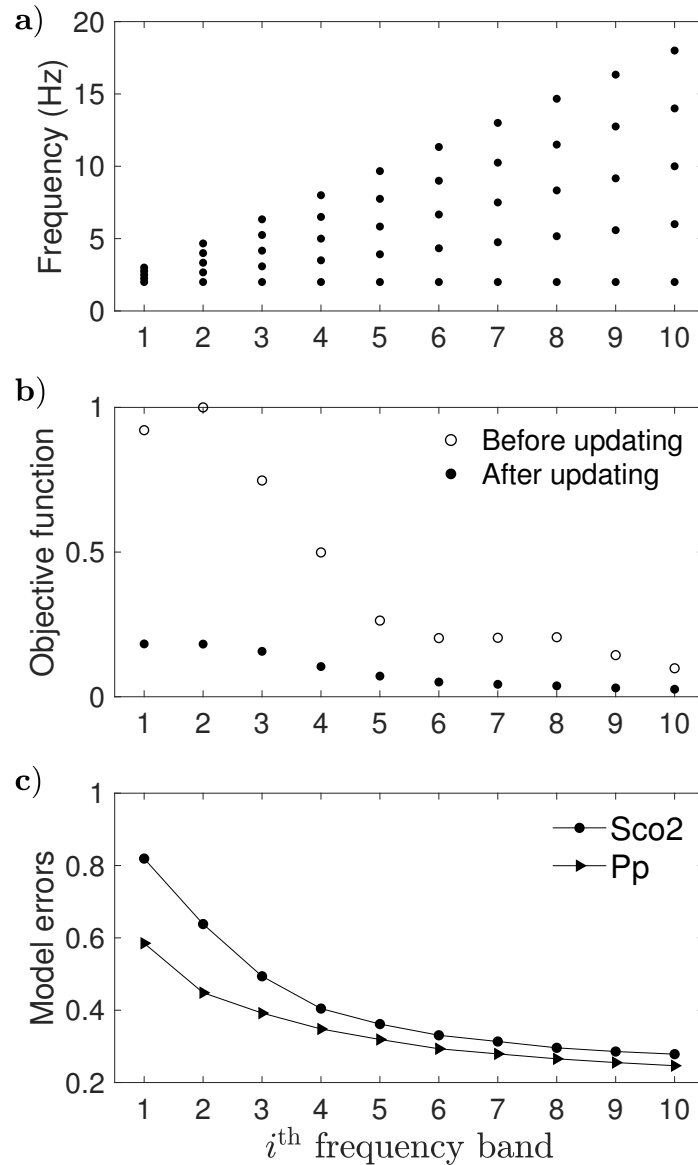


FIG. 10. Convergence properties. (a-c) Frequencies, objective functions, and model errors (after updating) within a frequency band, respectively.

REFERENCES

- Arts, R., Eiken, O., Chadwick, A., Zweigel, P., Van der Meer, L., and Zinszner, B., 2003, Monitoring of CO₂ injected at Sleipner using time lapse seismic data, *in* Greenhouse Gas Control Technologies-6th International Conference, Elsevier, 347–352.
- Batzle, M., and Wang, Z., 1992, Seismic properties of pore fluids: *Geophysics*, **57**, No. 11, 1396–1408.
- Bosch, M., Mukerji, T., and Gonzalez, E. F., 2010, Seismic inversion for reservoir properties combining statistical rock physics and geostatistics: A review: *Geophysics*, **75**, No. 5, 75A165–75A176.
- Brossier, R., Operto, S., and Virieux, J., 2009, Seismic imaging of complex onshore structures by 2D elastic frequency-domain full-waveform inversion: *Geophysics*, **74**, No. 6, WCC105–WCC118.
- Bunks, G., Saleck, F. M., Zaleski, S., and Chavent, G., 1995, Multiscale seismic waveform inversion: *Geophysics*, **60**, No. 5, 1457–1473.

- Chadwick, R., Arts, R., and Eiken, O., 2005, 4D seismic quantification of a growing CO₂ plume at Sleipner, North Sea, *in* Geological Society, London, Petroleum Geology Conference series, vol. 6, Geological Society of London, 1385–1399.
- Davis, T. L., Landrø, M., and Wilson, M., 2019, *Geophysics and geosequestration*: Cambridge University Press.
- Dupuy, B., Romdhane, A., Eliasson, P., and Yan, H., 2021, Combined geophysical and rock physics workflow for quantitative CO₂ monitoring: *International Journal of Greenhouse Gas Control*, **106**, 103,217.
- Eberhart-Phillips, D., Han, D.-H., and Zoback, M., 1989, Empirical relationships among seismic velocity, effective pressure, porosity, and clay content in sandstone: *Geophysics*, **54**, No. 1, 82–89.
- Grana, D., 2016, Pressure–velocity relations in reservoir rocks: Modified MacBeth’s equation: *Journal of Applied Geophysics*, **132**, 234–241.
- Grana, D., Mukerji, T., and Doyen, P., 2021, *Seismic Reservoir Modeling: Theory, Examples, and Algorithms*: John Wiley & Sons.
- Han, D.-h., 1987, *Effects of porosity and clay content on acoustic properties of sandstones and unconsolidated sediments*: Stanford University.
- Hu, Q., Grana, D., and Innanen, K. A., 2022, Predicting the time-evolution of co2 saturation through a combination of rock physics and full-waveform inversion, *in* SEG/AAPG International Meeting for Applied Geoscience & Energy, OnePetro.
- Hu, Q., Keating, S., Innanen, K. A., and Chen, H., 2021, Direct updating of rock-physics properties using elastic full-waveform inversion: *Geophysics*, **86**, No. 3, MR117–MR132.
- Jones, S. M., 1995, Velocities and quality factors of sedimentary rocks at low and high effective pressures: *Geophysical Journal International*, **123**, No. 3, 774–780.
- Keating, S., and Innanen, K. A., 2019, Parameter crosstalk and modeling errors in viscoacoustic seismic full-waveform inversion: *Geophysics*, **84**, No. 4, R641–R653.
- Landrø, M., 2001, Discrimination between pressure and fluid saturation changes from time-lapse seismic data: *Geophysics*, **66**, No. 3, 836–844.
- MacBeth, C., 2004, A classification for the pressure-sensitivity properties of a sandstone rock frame: *Geophysics*, **69**, No. 2, 497–510.
- Mavko, G., Mukerji, T., and Dvorkin, J., 2020, *The rock physics handbook*: Cambridge university press.
- Métivier, L., Brossier, R., Operto, S., and Virieux, J., 2017, Full waveform inversion and the truncated Newton method: *SIAM Review*, **59**, No. 1, 153–195.
- Pörtner, H. O., Roberts, D. C., Adams, H., Adler, C., Aldunce, P., Ali, E., Begum, R. A., Betts, R., Kerr, R. B., Biesbroek, R. et al., 2022, *Climate change 2022: impacts, adaptation and vulnerability*.
- Queißer, M., and Singh, S. C., 2013, Full waveform inversion in the time lapse mode applied to CO₂ storage at Sleipner: *Geophysical prospecting*, **61**, No. 3, 537–555.
- Ringrose, P., 2020, *How to Store CO₂ Underground: insights from early-mover CCS Projects*: Springer.
- Saul, M., and Lumley, D., 2013, A new velocity–pressure–compaction model for uncemented sediments: *Geophysical Journal International*, **193**, No. 2, 905–913.
- Sayers, C. M., 2006, Sensitivity of time-lapse seismic to reservoir stress path: *Geophysical prospecting*, **54**, No. 3, 369–380.